Live cell SERS imaging of intracellular pH: from 2D to 3D

Yizhi Zhang[‡†], *Dorleta Jimenez de Aberasturi**[†+], *Malou Henriksen-Lacey*[†+], *Judith Langer*[†] *and Luis M. Liz-Marzán**[†+Ɨ]

[‡]Advanced Photonics Center, Southeast University, 210096 Nanjing, China.

[†]CIC biomaGUNE, Basque Research and Technology Alliance (BRTA), Paseo de Miramón 182, 20014 Donostia-San Sebastián, Spain

[+]Centro de Investigación Biomédica en Red, Bioingeniería, Biomateriales y Nanomedicina (Ciber-BBN), Paseo de Miramón 194, 20014 Donostia-San Sebastián, Spain

[Ɨ]Ikerbasque, Basque Foundation for Science, 48013 Bilbao, Spain

*e-mail: djimenezdeaberasturi@cicbiomagune.es; llizmarzan@cicbiomagune.es

KEYWORDS. SERS imaging, intracellular pH, 3D imaging, pH probe, live cell imaging

ABSTRACT

Visualization of intracellular pH (i-pH) using surface-enhanced Raman spectroscopy (SERS) plays an important role toward understanding cellular processes including their interactions with nanoparticles. However, conventional two-dimensional (2D) SERS imaging often fails to take into consideration changes occurring in the whole cell volume. We therefore aimed at obtaining a comprehensive i-pH profile of living cells by means of three-dimensional (3D) SERS imaging, thereby visualizing dynamic i-pH distribution changes in a single cell. We devised herefore a biocompatible and highly stable SERS pH probe, comprising plasmonic gold nanostars functionalized with a pH-sensitive Raman reporter tag – 4-mercaptobenzoic acid (4MBA) – and protected by a cationic biocompatible polymer, poly-L-arginine hydrochloride (PA). The positively-charged PA coating plays a double role of enhancing cell uptake and providing chemical and colloidal stability in cellular environments. The SERS-active pH probe allowed visualization of local changes in i-pH, such as acidification during NP endocytosis. We provide evidence of i-pH changes during NP endocytosis via high-resolution 3D SERS imaging, thereby opening new avenues toward the application of SERS to intracellular studies.

Intracellular pH (i-pH) plays a highly relevant role in maintaining cellular metabolism and other cell functions. i-pH values in living cells are regulated within a range between 4 and 8, depending on the cell organelles and compartments, so that they accomplish their corresponding biological tasks.[1] Abnormal changes in i-pH are associated with cell dysfunction and may lead to diseases such as cancer.[2] Consequently, the development of sensitive and reliable i-pH sensors for disease monitoring and pharmaceutical treatments has gained exceptional interest.[3]

Among many currently existing i-pH detection approaches, surface-enhanced Raman spectroscopy (SERS) offers a number of advantages.[4–9] SERS appears superior to commonly used fluorescence microscopy in terms of its ultrasensitivity, multiplexing ability and high specificity, in addition to high photostability and low cytotoxicity.[8,10,11] Many advances have been reported on SERS imaging of i-pH in living cells.[6,12–15] However, they are consistently limited to analysis in two dimensions (2D). Despite the relatively rapid image acquisition in 2D, information in the vertical z axis has been sacrificed so far, meaning that a detailed i-pH profile in 3D has not been reported.

Recently efforts have been made to improve SERS-based 3D cell imaging from the micro to the macro level. Reports on the use of Raman imaging have focused on the 3D visualization of cell morphology and distribution of biomolecules,[16] as well as cellular endocytosis of SERS tags[17] or functionalized gold nanoparticles (AuNPs).[18] Our group has recently demonstrated SERS imaging of complex 3D multilayer cell models.[8] In these studies, however, cells were indispensably fixed to facilitate long-term 3D image collection, thereby losing the ability to obtain physiological information on live cells. With a focus on single NP tracking, Kawata *et al.* monitored the evolving SERS signals from AuNPs moving through a single cell in 3D, and more recently the pH dynamics tracking single NP transportation was obtained.[19–21] Herein, we propose that 3D SERS imaging is

indeed a suitable tool to provide an overall image of cells, by monitoring physiological parameters, such as pH, inside live cells.

We developed a pH-responsive plasmonic nanosensor comprising gold nanostars (AuNSs) as the plasmonic substrate, which are subsequently functionalized with the pH-sensitive molecule 4-mercaptobenzonic acid (4MBA), and externally wrapped with the cationic polymer poly-L-arginine hydrochloride (PA), as a protective layer. The resulting PA-engineered pH probes "AuNS-4MBA-PA" display high stability in relevant cellular oxidizing environments and at different pH conditions, while displaying excellent pH sensing performance. Biocompatibility and uptake efficiency were studied in a breast cancer cell line where endocytosis and the related i-pH changes could be monitored using SERS. We explored first the use of 2D SERS imaging in live cells, and then high-resolution 3D SERS imaging to obtain more detailed and precise information with sub-cellular resolution, of i-pH in living cells.

RESULTS AND DISCUSION

Polyarginine-engineered pH SERS probe

A reliable SERS nanoprobe for monitoring i-pH in live cells should meet some essential requirements. Apart from biocompatibility required for live-cell imaging, this probe should be sensitive to a near infrared (NIR) excitation laser source to avoid cellular autofluorescence and reduce phototoxicity. Additionally, fast and reversible responses to pH changes are needed for dynamic i-pH sensing. The probe should be highly stable in the intracellular microenvironment, thereby meeting the requirements of long-term cell culture. Finally, it is important to use bright SERS nanoprobes, which display high cell-uptake efficiency, to ensure fast and accurate 3D imaging. Commonly used pH sensitive Raman reporters (RaRs), including 4MBA,[12,13,21–24] 4-

mercaptopyridine,[6,14,15] and para-aminothiophenol,[26] among others, are often hydrophobic. The combination of such molecules with a SERS-active AuNP would thus inevitably lead to colloidal instability and aggregation, especially in complex solutions with high ion and protein concentration such as cell culture media.[27,28] Protective layers such as silica shells are unfavorable for studies requiring long-term exposure to cell media due to degradation and agglomeration issues.[29–31] Commonly-used thiolated polyethylene glycol (PEG) can compete with pH-RaRs in the NP surface binding process, resulting in decreased signal intensity and reduced pH detection limit.[5] Other layers possessing negative surface charge, such as bovine serum albumin (BSA), can result in a low level of NP cellular internalization.[32]

Thus, to achieve accurate i-pH measurements and long-term observations, we developed a pH-sensitive SERS probe protected by a layer of the cationic polymer PA. PA is an arginine-rich polypeptide, which has been preferentially used in gene delivery and transfection since it carries high net positive charge and can therefore associate via electrostatic interactions with the cell membrane and translocate into the cytosol.[33] Conjugating PA on cargos, such as proteins, quantum dots, nucleic acids etc. or on negative nanoparticles like silica or carbon nanotubes, facilitates their endocytosis and translocation in cells.[34] It has been additionally shown that PA-coated NPs are more efficiently taken up by cells.[8] In our case, this layer is expected to play various important roles in the behavior of the resulting nanosensor: (i) it provides colloidal stability in different media; (ii) it provides biocompatibility to the probe; (iii) it increases the cellular internalization efficiency. Additionally, the permeability of the PA layer facilitates the diffusion of ions from the outer medium, thereby allowing the change of the 4MBA protonization state under different local pH.

Our pH-sensitive SERS probes were prepared as illustrated in **Figure 1A**. AuNSs were synthesized by means of the surfactant-free method[35] and subsequently modified with 4MBA (~20 molecules/nm^2), which can readily adsorb onto the AuNS surface via thiol-gold covalent bonding. 4MBA-conjugated AuNSs (AuNS-4MBA) were then added dropwise to a solution of PA (~0.5 mg per μmole of Au^0), which rapidly wraps around negatively-charged AuNS-4MBA due to electrostatic interactions (the conditions for surface modification are summarized in **Table S1**). The obtained structure (average tip-to-tip diameter = 52.0±7.0 nm) can be determined using transmission electron microscopy (TEM), as exemplified in **Figure 1B**. Upon functionalization of AuNSs with 4MBA and the protective PA shell, the localized surface plasmon resonance (LSPR) band was observed to red-shift by 27 nm and 38 nm, respectively, from those of the initial AuNSs, due to changes in the dielectric environment around the metal surface[36] (**Figure 1C**). Importantly, no LSPR broadening was observed, indicating that AuNSs remain stable during the various functionalization stages. Dynamic light scattering (DLS) characterization revealed only a slight increase (~6 nm in the dominant peak) in the average hydrodynamic diameter of AuNSs after 4MBA functionalization, in agreement with its rather small size (MW = 154.19 g/mol), while a larger increase of ~22 nm was determined after encapsulation with PA (molecular weight > 70k) (**Figure 1D**). One should note that the small peak at ca. 6 nm in Figure 1D refers to the rotational diffusion coefficient of AuNSs, recorded in DLS measurements. Additionally, the final addition of PA resulted in a reversal of the zeta potential from -23.3 mV to +33.5 mV (**Figure 1E**). All changes observed thorugh various characterization tools were indicative of a successful AuNS surface functionalization with PA and uniform coverage of the particles.

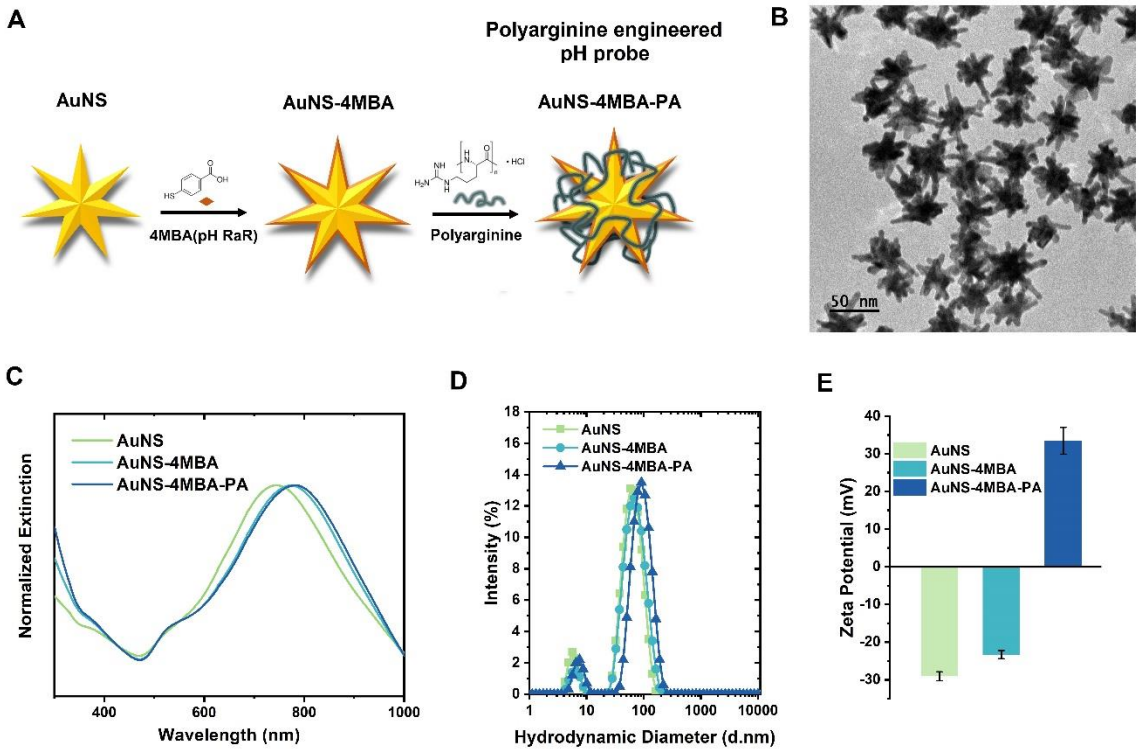

Figure 1. A) Schematic illustration of the stepwise synthesis of PA-engineered pH probes (AuNS-4MBA-PA): AuNS are functionalized with 4MBA (pH-RaR) and then wrapped with PA. B) Representative TEM image of AuNS-4MBA-PA. C-E) UV-vis spectra (C), hydrodynamic diameter distributions (D), and average zeta potential (E) for AuNS, AuNS-4MBA and AuNS-4MBA-PA.

Stability of AuNS-4MBA-PA nanosensor

An essential requirement for NPs to be used as intracellular sensors is high stability within complex biological systems. NP-based sensors that will be used for measuring i-pH should be stable in cell culture media, prior to cellular internalization. Such a high stability should also remain within an intracellular oxidative environment, e.g. due to the generation of reactive oxygen species (ROS),[37,38] which are known to have etching or oxidizing effects on AuNSs.[39–41] One should also be aware that metallic nanoparticles themselves can mediate an excessive production of cellular ROS, resulting in oxidative cellular stress and leading to cell toxicity.[42] We focus the

discussion here on the stability of pH SERS probes against oxidizing agents, while NP-induced cell toxicity will be discussed below.

Aiming to simulate oxidizing conditions, AuNS-4MBA-PA were exposed for 24 h to two different ROS, hydrogen peroxide (H_2O_2, 0.1% w/w) and sodium hypochlorite (NaClO 0.1% w/w). In order to evaluate the stabilizing effect of the protective PA layer, AuNS and AuNS-4MBA precursor stages were also tested for comparison. To challenge and ensure stability under real conditions, the concentrations used in these experiments were approximately 1000-fold higher than those typically found in cells (usual intracellular concentrations are in the μM range).[38,43] To follow the evolution of AuNS LSPR, time-dependent UV-vis measurements were recorded over 24 h, with a resolution of 10 min, and the results are summarized in **Figure 2**. Under H_2O_2 exposure (**Figure 2A**), the precursor AuNSs show a LSPR blueshift of ca. 40 nm within a timeframe of 24 h, which indicates a minor and slow modification of the AuNS morphology. On the other hand, a much smaller LSPR blueshift of ca. 20 nm in AuNS-4MBA shows that functionalization with 4MBA significantly hinders AuNS reshaping and thus contributes to the stabilization of the synthesized probe. This effect is likely due to covalent binding of 4MBA, which limits the mobility of Au atoms on the AuNS surface.[36,44] The stable position of the LSPR maximum, combined with a minor variation in the extinction intensity (**Figure S1**) for AuNS-4MBA-PA probes, indicates that the protective PA layer provides a more pronounced long-term stability against exposure to a high-concentration of H_2O_2.

A different result was obtained under the oxidizing effect of NaClO at high concentration, which was found to degrade both unprotected and protected AuNSs, likely due to its higher oxidation potential against Au.[39,45] **Figure 2B** shows a steep decay of the extinction signal at 400 nm, which reaches half the initial value after ca. 300 min, for unprotected AuNSs. The gradual and complete

damping of the LSPR band (**Figure S1**) points to a rapid dissolution of AuNSs upon oxidation and/or precipitation, which can also be observed by eye through color loss in the solution. Notwithstanding, the presence of the PA protective layer significantly slows down the precipitation/dissolution rate of AuNSs during the first 800 min. It is also worth mentioning that, at milder oxidation conditions (100 μM NaClO), the PA-protected SERS probe is slowly and partially precipitated over 24h but the initial LSPR spectrum is recovered after sonication (**Figure S2**). Under the same conditions, unprotected AuNS-MBA are partially precipitated but additionally show a small blueshift of 10 nm, indicating a subtle morphology change at AuNS tips (**Figure S2D**), whereas naked AuNSs are largely degraded and reshape into sphere-like structures. We thus conclude that the PA layer efficiently protects the pH SERS probe during our experimental time window, even in the presence of highly aggressive oxidizing agents.

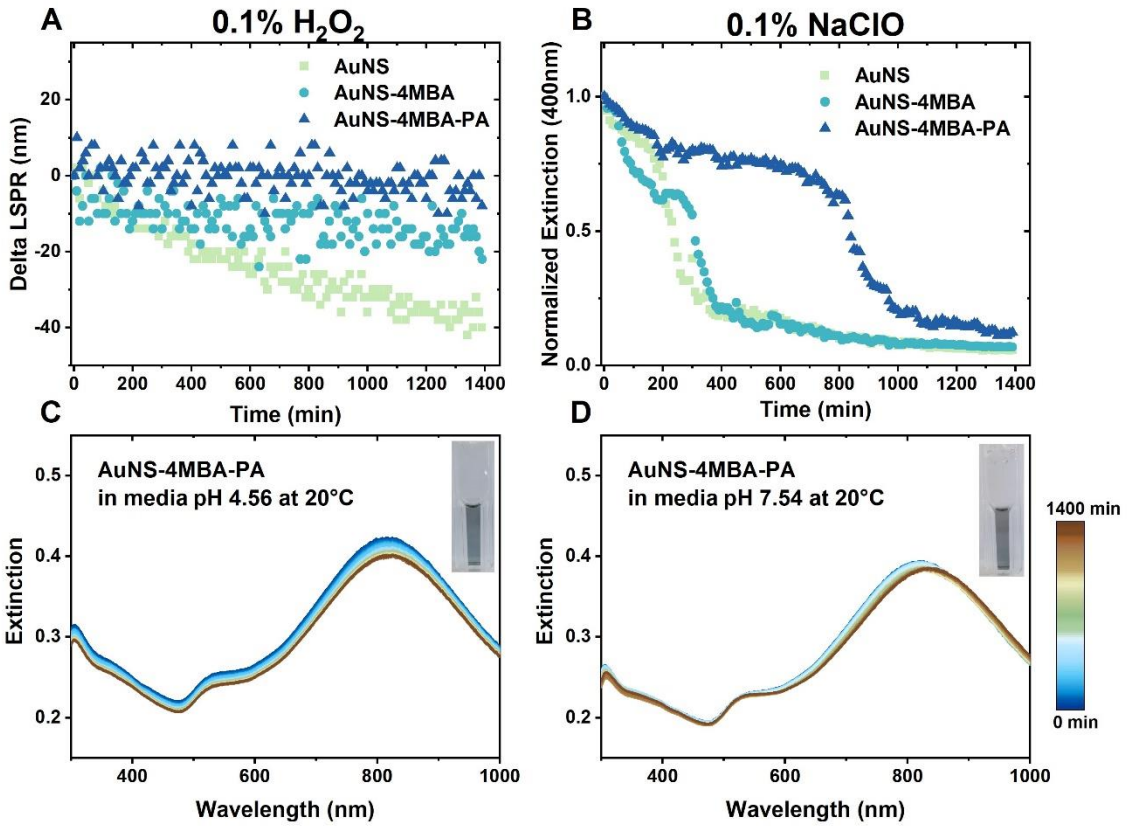

Figure 2. UV-vis spectroscopy analysis of nanoparticle stability within 24 h at 10 min intervals. A) Time trace analysis of AuNS, AuNS-4MBA and AuNS-4MBA-PA suspended in 0.1% w/w H_2O_2. B) Equivalent analysis in 0.1% w/w NaClO. Time traces of normalized LSPR peak shifts are displayed in (A), whereas the normalized extinction at 400 nm is plotted in (B). C,D) Real-time UV-vis spectral traces (at 20 ℃) for AuNS-4MBA-PA in cell culture media supplemented with 10% FBS at pH 4.56 (C) and at pH 7.54 (D). Insets are the photographs after incubation for 24 hours.

We next investigated the colloidal stability of AuNS-4MBA-PA in cell culture conditions. AuNS-4MBA-PA were incubated for 24 h in cell culture media containing 10% v/v fetal bovine serum (FBS). Two different pH conditions were considered – 4.56 and 7.54 – which mimic lysosomal and extracellular environments, respectively. The time evolution of the UV-vis spectra shows a slight decrease in extinction (~4.6%) during incubation in media at pH 4.56, whereas a subtle LSPR redshift (~12 nm) was observed when incubated at pH 7.54 (**Figure 2C and D**). The observed decrease in absorbance might result from imperceptible nanoparticle precipitation, whereas the LSPR shift may arise from the temporal evolution of various components present in media, such as proteins,[46,47] which can readily adsorb onto the surface of AuNPs.[48] An increase in absorbance was observed in both cases (pH 4.56 and 7.54), when the incubation in media was performed at 37 ℃ (**Figure S3A and B**), in agreement with previous reports for quasispherical AuNPs.[48] The increasing extinction can also be attributed to changes in the profile of protein adsorption on the AuNP surface, which is likely to affect the complex dielectric function near the interface between NPs and solvent.[48]

pH sensing with AuNS-4MBA-PA

The pH sensitivity of AuNS-4MBA-PA was tested in pH-modified cell culture media containing 10% v/v FBS, thereby simulating biological conditions with high concentrations of proteins, ions

and other molecules.[15,23,49] The pH of complete cell media (i.e., cell media containing 10% FBS and 1% penicillin-streptomycin) was adjusted through the addition of HCl or NaOH, and the exact pH was confirmed using an electronic pH meter. The status of NPs in media was interrogated by DLS (**Figure S4**) to confirm their colloidal stability. Normalized SERS spectra from AuNS-4MBA-PA in the various pH media are shown in **Figure 3A**. The pH-associated Raman peak, located around 1420 cm^{-1}, is assigned as the COO- stretching mode.[5] By deconvoluting the band ranging from 1370 to 1470 cm^{-1} (**Figure S5**), this peak was first detected at 1415 cm^{-1}, whereas at increasing pH a minor increase in intensity and a redshift to 1429 cm^{-1} were observed, which is in agreement with other reports.[2,23] It has been reported that the band at 1415 cm^{-1} corresponds to surface-bonded COO- groups with intramonolayer bonding, whereas the peak at 1429 cm^{-1} is assigned to unbound COO- groups in 4MBA, which display a more vertical orientation pointing away from the gold surface.[50] Therefore, considering they are both involved in the process of 4MBA deprotonation, we used the ratio between the sum of these two bands (1415 and 1429 cm^{-1}) and the strongest peak at 1081 cm^{-1} (attributed to benzene ring breathing and axial deformation[5]) as the indicator for pH measurement.[1] The intensity ratio is plotted versus pH in **Figure 3B**, which is found to follow the expected trend from Henderson-Hasselbalch equation.[2] By fitting the data, we obtained the following correlation, which serves as the calibration curve to quantify i-pH (R denotes the intensity ratio between SERS peaks).

$$pH = 5.895 + log_{10}\frac{R-0.058}{0.251-R} \quad (r^2 = 0.96)$$

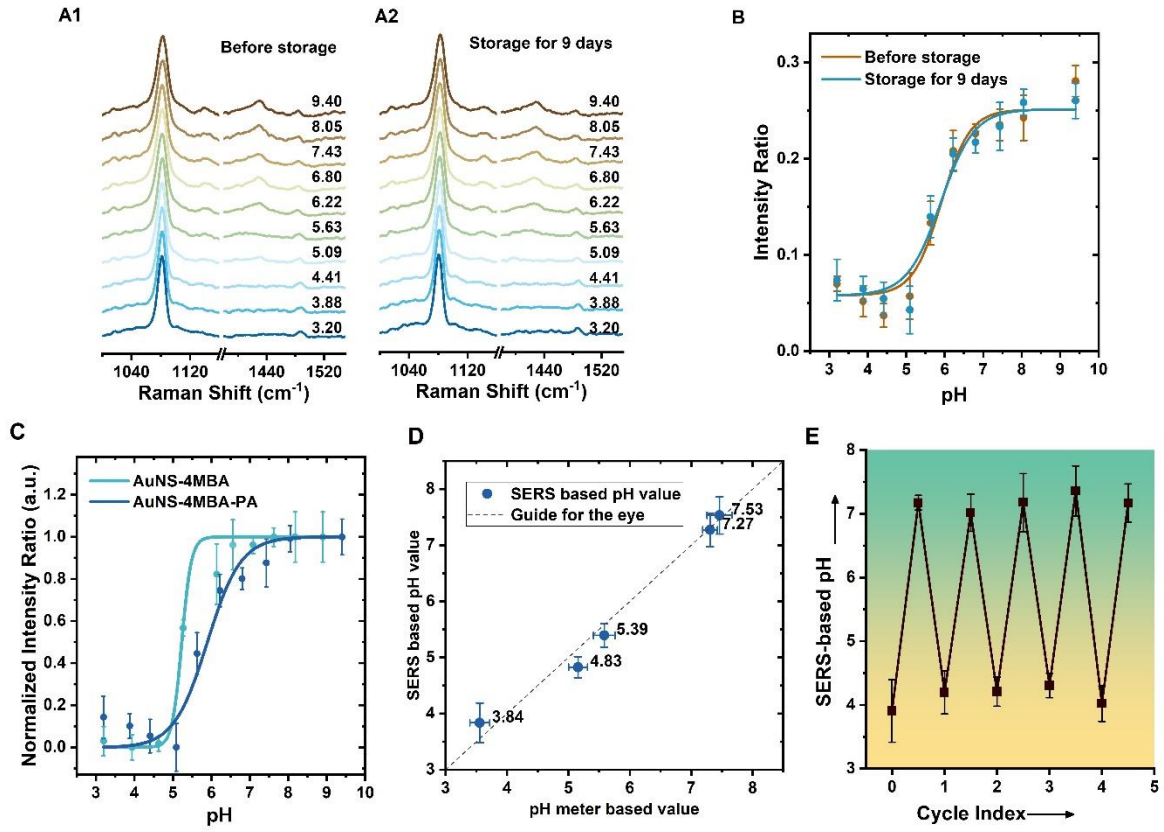

Figure 3. A) Normalized SERS spectra of AuNS-4MBA-PA in complete cell culture media with different pH, before (A1) and after (A2) storage for 9 days. B) Calibration curves obtained before and after storage, by determining pH values with an electronic pH meter. Each spectrum is the average of 5 measurements. C) Normalized pH response curves using pH probes with and without polyarginine (AuNS-4MBA-PA and AuNS-4MBA). D) Recall test of pH sensing using SERS with AuNS-4MBA-PA and an electronic pH meter (the dashed line is a guide for the eye to show linearity). E) Reversible pH switching measured with AuNS-4MBA-PA in water. pH was adjusted by addition of HCl or NaOH. Error bars show the standard deviation from three measurements.

A comparison with the calibration curve for the probe without PA coating (**Figure 3C**) shows a sharper and narrower working range (pH 5-6) for the latter. Therefore, AuNS-4MBA-PA appear more suitable for i-pH measurements, as a result of a relatively gentle slope in the working pH range between ca. 4 to 8, which covers the physiological pH in cells. This shift of the pH response curve is attributed to the effect of the PA layer, which can affect the diffusion behavior and

dynamics of ions (in particular protons), from the medium to the AuNS surface or/and due to changes in the orientation of 4MBA molecules when wrapped with PA at the nanoparticle surface.[13,51] After nine days of storage at 4 °C, the morphology, SERS spectra and pH sensitivity of the probes were preserved (**Figures S6A, S6B, 3A2** and **3B**), which again demonstrates high colloidal stability in cell media and sensing stability. We additionally examined the reproducibility of the pH response curve among three different batches of AuNS-4MBA-PA (**Figure S6C**), as well as a recall test and a cyclic test, to investigate their accuracy and reversibility. The pH values of the media obtained by SERS measurements were validated with an electronic pH meter (**Figure 3D**). **Figure 3E** shows an example of cyclic pH sensing by AuNS-4MBA-PA, confirming that similar pH values were determined when the pH was subjected to five consecutive sensing cycles. Given the observed variations in the extinction spectra when incubating the probe in warm media (**Figure S3A and B**), it is important to verify that the pH response is not influenced by protein adsorption or AuNS aggregation. SERS spectra were thus recorded at different incubation times in media at 37 ℃, for 24 hours, in which the pH-dependent intensity ratio was found to remain constant at both pH 4.56 and 7.54 (**Figure S6D**). These results indicate that the probe can preserve its pH sensing ability in both acidic and basic biological complex media for at least 24 h, thereby providing reliability toward intracellular pH sensing.

Cellular uptake and biocompatibility

Prior to investigating i-pH in living cells, we first studied the biocompatibility and internalization in the MCF7 breast cancer cell line, using our PA-coated SERS probe as compared to more standard biocompatible PEG-coated SERS nanosensors.[52] Results based on the MTT assay (**Figure 4A**) for both coating shells at 2 - 50 μg/mL concentrations show no significant alterations

in cell viability, which consistently exceeds 85%, even for the highest dose. We additionally studied the level of uptake for both nanosensors employing inductively coupled plasma-mass spectrometry (ICP-MS) quantification and SERS imaging. **Figure 4B** clearly shows that cellular internalization of PA-coated probes increases with the applied dose, compared to PEG-coated probes, reaching uptake levels between 27% (for 2 μg/mL) and 52% (for 50 μg/mL). Further support in the same direction is provided by both bright-field optical microscopy (**Figure S7**) and SERS mapping (**Figure 4C**). The much higher contrast provided by the PA-coated probe (**Figure S7** right) compared to PEG-coated SERS nanosensors (**Figure S7** left) confirm the much higher accumulation of AuNS-4MBA-PA probes in MCF7 cells. As a result, a strong SERS signal can be collected over the cell area for the 4MBA marker when using AuNS-4MBA-PA (**Figure 4C** left), whereas PEG-coated AuNS-4MBA yield a weak signal intensity, spotted at few places (**Figure 4C** right). In summary, when compared with typically used PEG-coated pH sensors at the same concentration, the encapsulating PA layer endows pH SERS probes with excellent cell loading ability and high biocompatibility toward MCF7 cells.

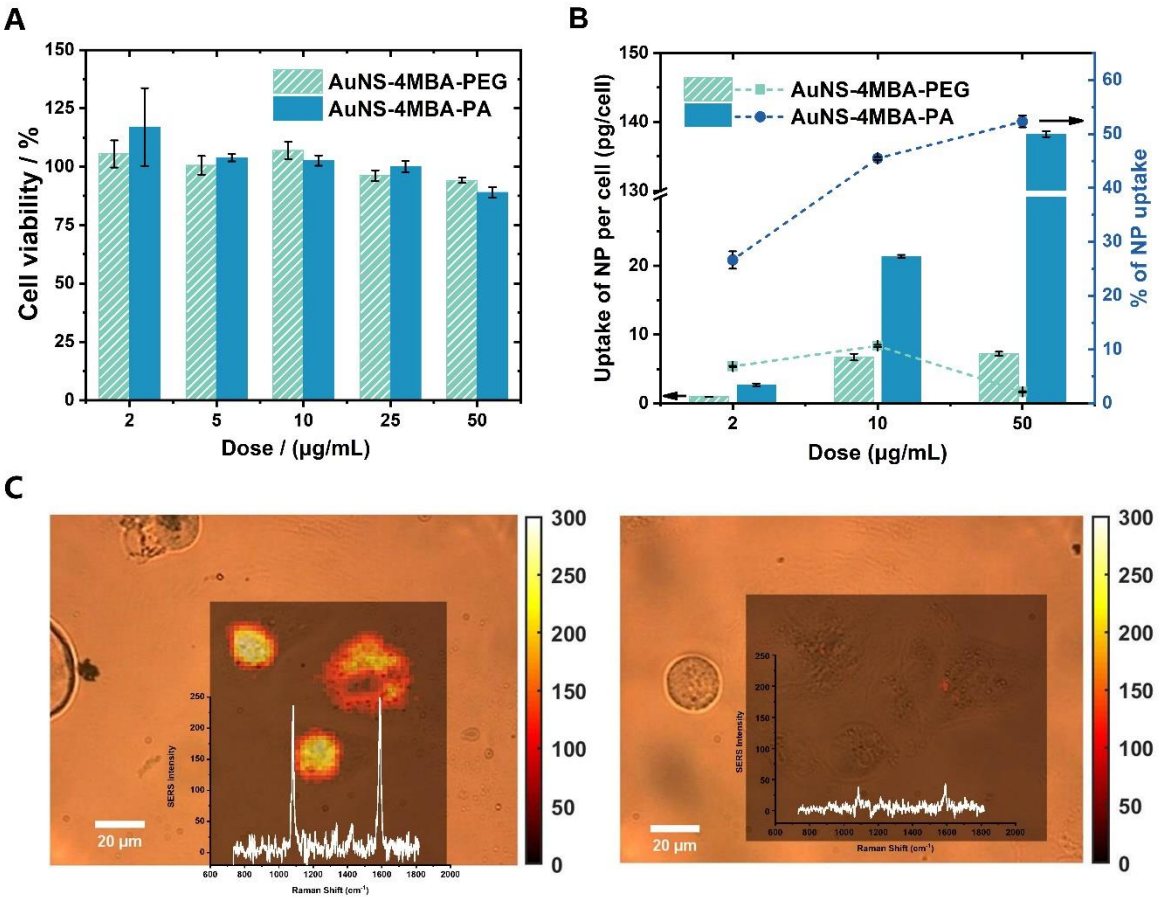

Figure 4. Comparison of MCF7 cell viability and NP uptake for PA-coated and PEG-modified pH probes (AuNS-4MBA-PA and AuNS-4MBA-PEG, respectively). A) MTT assays for cells incubated overnight with different doses of both NPs. B) Quantification of cellular uptake of AuNPs per cell (pg/cell) and mass percentage of Au (%) internalized by cells (dotted and dashed lines, respectively), after 24 h incubation determined by ICP-MS. C) Merged SERS intensity at 1081 cm^{-1} and bright-field images of MCF7 cells exposed to 10 μg/mL of AuNS-4MBA-PA (left) and AuNS-4MBA-PEG (right). The insets are representative spectra from the SERS images.

2D Time-lapse i-pH sensing

It is well-known that, during the process of cellular endocytosis, NPs are exposed to environments in which there are significant variations in pH.[1,53] NPs are exposed to initial pH values of approximately 6 – 7 during the first stage of endocytosis. As endocytic vesicles move

inwards to the perinuclear area and fuse with lysosomes, pH decreases down to 5 – 6. More acidic pH (4.5 – 5) can also be reached when NPs-containing vesicles are completely matured.[54,55] Encouraged by the reliability and high cellular uptake level of AuNS-4MBA-PA, we carried out i-pH sensing coupled to 2D SERS imaging. MCF7 cells were thus exposed to AuNS-4MBA-PA NPs for 2h and washed to remove non-endocytosed NPs (**Figure 5A**). The first SERS mapping was performed immediately after NP removal (2 h, leftmost column in **Figure 5B**), followed by successive mappings every 2h. As excess SERS probes were removed after the first 2h of incubation, the SERS probe concentration should not increase after recording the first image. By this procedure, we can track changes in the distribution and localization, as well as in the chemical environment, of the initial NP population. **Figure 5B** displays bright field, SERS intensity and pH-constructed images of two MCF7 cells. The images depict the gradual translocation of NPs from the cell membrane into the perinuclear area, which is a common feature of NP endocytosis.[56] Interestingly, the false-coloured pH maps are in agreement with the expected pH variations with time and location; for instance, perinuclear pixels at 8 h appear more yellowish (i.e. more acidic) than they are at 2 h, when they are close to the cell membrane. These results indicate an accumulation of SERS probes inside acidic vesicles at late stages of endocytosis.

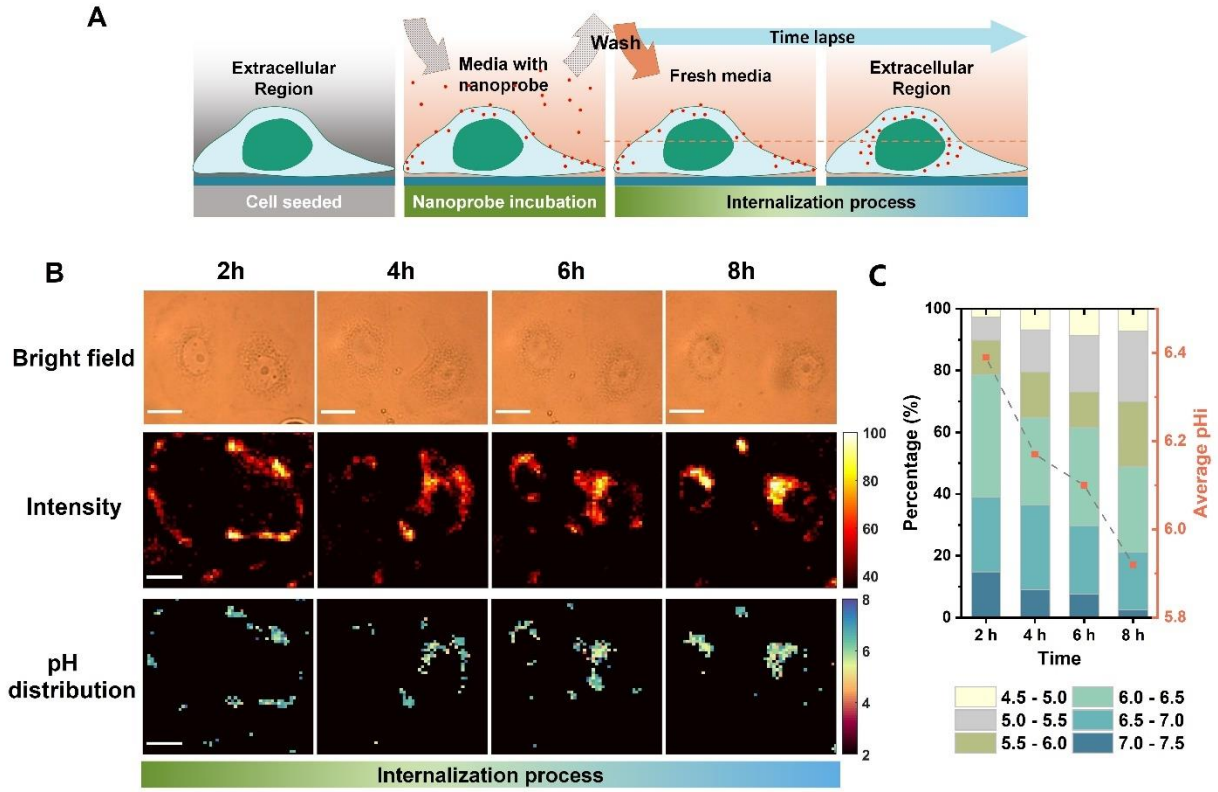

Figure 5. Time-lapse pH monitoring of two MCF7 cells during the internalization of AuNS-4MBA-PA. A) Schematic description of the experiment. B) Bright field, SERS mapping, and pH distribution maps of two live MCF7, after 2h of incubation with 10 μg/mL AuNS-4MBA-PA in cell culture media, followed by replenishing with fresh media. SERS measurements were conducted with a 785 nm laser using *streamline mode*. Each image takes ca. 5 min. SERS intensity images were generated with the intensity at 1081 cm^{-1} and the pH distribution was constructed using the calibration curve in Figure 3. Scale bars are 20 μm. C) Percentage of pixels in a certain pH range from the overall valid pixels, at specified time points. A dot and line chart (orange square dot and dashed line) displays the average local pH at different time points.

To better demonstrate the data, we plotted against each other the percentages of pH values falling within different pH ranges, representative of specific subcellular compartments, in the form a stacked bar graph (**Figure 5C**). As previously reported, lysosomal vesicles are the most acidic cellular organelles, expressing pH values in the range of 4.5 – 5.0.[1,51] Endosomes are less acidic

and include late endosomes (pH 5.0 – 6.0), early endosomes (pH 6.0 – 6.5) and recycling endosomes (pH 6.5 – 7.0), while the pH of cytosol, endoplasmic reticulum and the extracellular area are within the range of 7.0 – 7.5.[1] As shown in **Figure 5C**, 80% of pixels were identified in the pH range of 6.0 – 7.5 at the initial time point (2 h). As expected, the local pH experienced by AuNS-4MBA-PA becomes more acidic over time, with the proportion of detected pH values below 6 being doubled at the latest observation time (8 h). Although the proportion of pixels with pH 7.0 – 7.5 in the whole map was found to gradually decrease over time, a few such pixels could be observed after 8 h. We propose that this may partly arise from either residual AuNSs on the culture dish or a potential endosomal escape of AuNS-4MBA-PA, as previously described for other positively charged NPs.[54,56] To obtain more information regarding the initial exposure of cells to NPs, we carried out an additional experiment where the incubation time was shortened down to 15 min (**Figure S9**). It should be noted that the concentration of AuNS-4MBA-PA had to be increased to obtain a sufficient probe signal, to overcome the detection threshold at such early time points. Unlike the previous experiment, no highly acidic pH values (4.5 – 5.0) were detected at the initial 15 min time point, meaning that the probes have not gone through complete maturation of endosomes within the short 15 min period.[55]

3D time-lapse observation of nanoparticle internalization and intracellular pH

Whilst 2D imaging provides information on i-pH changes in the same plane, the use of 3D z-stack SERS imaging helps gathering a more in-depth understanding of NP dynamics in an individual cell. For 3D imaging, MCF7 cells were exposed to AuNS-4MBA-PA for 2 h, followed by washing and replenishment with fresh cell media. Considering the longer time required for 3D imaging, we decided to restrict the measurements to imaging the cell at the first and last time

window. An additional compromise was made on signal intensity and imaging time, to reduce any possible optical and thermal damage to the cell. Bright field images pre- and post-imaging at both time points, confirmed no laser-induced cytotoxicity (**Figure S10**). The SERS intensity from AuNS-4MBA-PA probes was thus reconstructed in various slices of the z-stack shown in **Figure 6A**. The 3D localization of the SERS nanoprobes within the cell at both time points, corresponding to 2 and 8 h, can be reconstructed from the 2D images of levels 3-5, which agrees roughly with the volumetric height of a live MCF7 cell (ca. 6-8 μm).[57] Despite of the limited resolution in z, the positional information of AuNS-4MBA-PA in the cell at both time points supports our main findings from 2D studies, i.e. the motion of NPs from cell membrane-associated locations toward the perinuclear area of the cell (**Figure 6B**). These results are also in line with the plot of integral signal intensity on the lines drawn across the image, along the x and y axes (**Figure 6C and D**). We plotted the number of pixels in each layer with distinct SERS intensity at 1081 cm^{-1} vs. the z-height, thereby visualizing the preferential locations of NPs within the cell (**Figure 6E**). These results suggest that, prior to endocytosis, most of the SERS probes are present at the lowest layer of the cell (5^{th} layer, 2 h), in contact with the underlying culture dish. After endocytosis, NPs are seemingly concentrated around the middle layer (4^{th} layer, 8 h), which supports the observation of NP accumulation in the perinuclear region. In addition to AuNS-4MBA-PA probe location, the pH sensitivity of the probe allowed us to determine the local pH from the vibrational spectra. In **Figure 6F**, we selected 3 different points for each time point (2 h and 8 h) where a large number of SERS probes have accumulated (brightest areas), and then analyzed the molecular fingerprint spectra. This selection suggests that some intracellular areas display a lower pH after 2 h (5.61 at point 2) than points selected near the cell membrane (6.54 and 7.10 at points 1 and 3 in **Figure 6F** left). We thus conclude that a small fraction of NPs was internalized and endosome maturation

occurred at the earliest time point. As expected, after 8h all selected points at perinuclear locations show acidic values (in the range of 5 to 6 at three selected points in **Figure 6F** right).

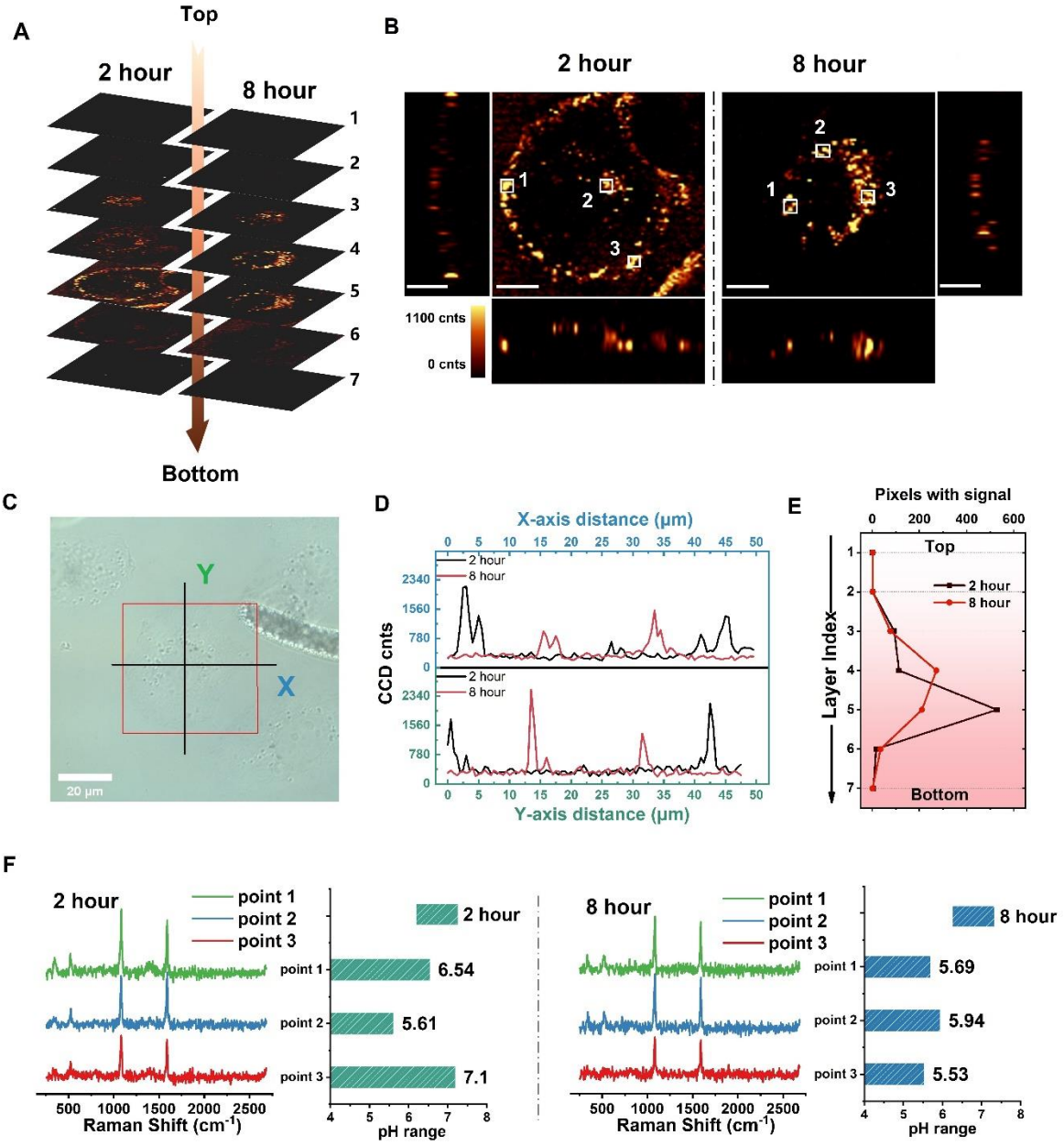

Figure 6. Reconstruction of 3D SERS imaging. A) Stacked slides for 3D SERS imaging at time points 2 h and 8 h, on the same cell (also shown in C). SERS images measured with a spatial step size of 0.5 μm in x-y and an interval distance between each layer of 2 μm. B) Orthogonal view of the z-stacks shown in A), with the main xy image showing the 5th and 4th layers of the 2 h and 8 h

time-points, respectively. Scale bars: 10 μm. C) Bright field microscopy image of the observed cell prior to imaging. D) Overlapped integral signal intensity in the lines drawn on C, along x and y. E) Number of pixels with signal in each layer. F) Average spectra from squares 1, 2 and 3 in B), and their corresponding pH.

Finally, by grouping the common pH values of each pixel, we can find distinct pH distributions in each layer (**Figure 7**). Consistent with the initial intensity profiles (**Figure 6E**), most pH pixels present at the lowest part of the cell (5^{th} layer after 2 h) are subsequently located at the middle part (4^{th} layer after 8 h). Such pH range groups provide information that cannot be observed in 2D maps. For example, those pixels corresponding to a detected pH above 7.0 only appear at the lowest part of the cell at 2h; whereas some are found at the top layers of the cell after 8h. The presence of such basic pH pixels at the latter time point may indicate NP escape from endosomes into the cytoplasm, or even exocytosis of NPs by the cell. Furthermore, most pixels with pH values below 6 at 8 h are concentrated in the middle layer of the cell, revealing a dramatic increase compared to the earlier time point, in agreement with the expected acidification during endocytosis.

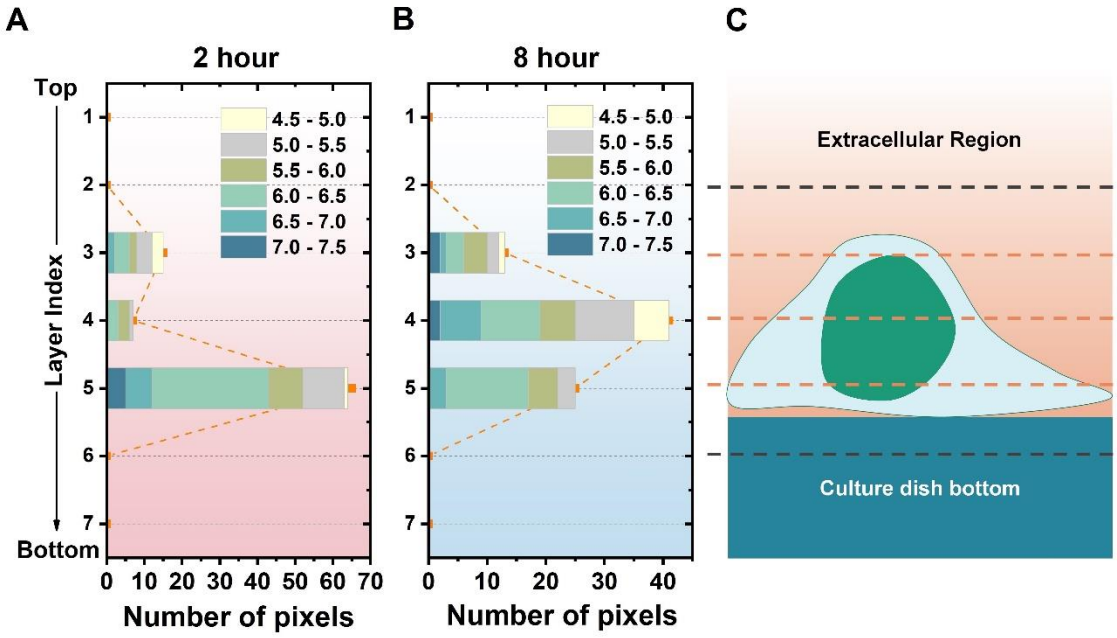

Figure 7. Analysis of the pH range distribution as a function of pixel number in different cell levels. A,B) Stacked column representation for the time points 2 h (A) and 8 h (B). Data were obtained from SERS scans shown in Figure 6A. C) Illustration of the imaged cell and the corresponding scanning Z-positions in the cell (dashed lines).

Conclusions

In summary, we devised and fabricated stable and highly biocompatible plasmonic SERS pH probes, that allow reliable visualization of 2D and 3D intracellular pH. By employing a cationic polymer as the outmost wrapping layer around pH-sensitive SERS tags, colloidal stability, cellular internalization efficiency and biocompatibility were largely improved. Using MCF7 breast cancer cells as a model, we observed by 2D SERS imaging the local pH acidification during NP endocytosis. We have additionally presented proof-of-concept 3D SERS imaging of pH changes during NP endocytosis in individual live cells. NPs were observed to accumulate at perinuclear locations, and the associated local decrease in pH indicated diffusion from endosomal to lysosomal

compartments. We envisage that these SERS i-pH probe and high-resolution 3D SERS imaging method will allow in the future to dynamically track pH variations at the single-particle level during endocytosis, or even to map pH distributions within complex 3D mammalian cell culture models.

METHODS

Materials. Milli-Q water (resistivity 18.2 MΩ·cm at 25 °C) was used in all experiments. Hydrogen tetrachloroaurate trihydrate ($HAuCl_4 \cdot 3H_2O$, ≥99.9%) was purchased from Alfa Aesar. L-ascorbic acid (≥99%), sodium hydroxide, sodium hypochlorite solution, silver nitrate ($AgNO_3$, ≥99%), sodium citrate tribasic dihydrate (≥98%), poly-L-arginine hydrochloride (PA; Aldrich # 26982-20-7>70,000Da), O-[2-(3-mercaptopropionylamino)ethyl]-O'-methylpolyethylene glycol (PEG-SH, MW=5000 g/mol), 4-mercaptobenzoic acid (4MBA, 99%), and hydrogen peroxide (H_2O_2, 28%), were supplied by Sigma–Aldrich. Hydrochloric acid (37 wt %) was purchased from Panreac.

Synthesis of gold nanostars. Surfactant-free AuNSs were synthesized as previously reported.[35] Briefly, 15 nm Au seeds were prepared by the classic Turkevich method. Au concentration was determined by UV-vis spectroscopy from the absorbance at 400 nm. 0.1 mL of 0.125 M $HAuCl_4$ solution and 0.05 mL of 1 M HCl were sequentially added to 50 mL of nanopure water. Then 2.5 mL of Au seed solution ([Au] = 0.53 mM) was added at room temperature under vigorous stirring. Afterwards, using two 1 mL pipettes for simultaneous addition, 500 μL of 3 mM $AgNO_3$ and 250 μL of 100 mM ascorbic acid were added, simultaneously and quickly. The solution color rapidly changed from light red to bluish, indicating the formation of nanostars. In order to stabilize AuNSs, 100 μL of 0.1 mM PEG-SH (~0.25/nm^2) was added under moderate stirring for 10 min. After

centrifugation at 6500 rpm for 15 min, AuNSs were suspended in water and stored at 4 ℃. The size of as-synthesized AuNSs was 52.0±7.0 nm from tip to tip. LSPR maximum was located at 782 nm.

Synthesis of AuNS-4MBA-PA. 8 mL of as-synthesized AuNSs ([Au^0] = 0.5 mM) was gently stirred in a 15 mL glass vial. 1 mL of 0.16 mM 4MBA solution was added and stirred for 30 min. The number of added RaR molecules was calculated to be ~20 molecules per nm^2 . The footprint of 4MBA has been reported to be ca. 3 molecules/nm^2.[51,58] Therefore, the amount of 4MBA added to the NPs was calculated using a 7-fold excess (20 molecules/nm^2) to reach a complete monolayer. The excess of 4MBA was then removed by washing the NPs by centrifugation. The mixed solution was then added dropwise to 2 mL of 1 mg/mL polyarginine solution, under vigorous stirring. After 2 h, the solution was washed twice by centrifugation at 3000 rpm for 10 min. As a comparison in cellular uptake quantification, AuNS-4MBA-PEG was synthesized by mixing 150 μL of 0.1 mM PEG-SH (~2/nm^2) for 30 min, after 4MBA modification.

Chemical stability evaluation. The stability test was performed with 1 mL colloidal solution ([Au^0] ≈ 0.1 mM) by a Cary 3500 Multizone UV-vis spectrophotometer (Agilent Technologies, Inc.) for 24 h. 0.1% w/w NaClO, 0.1% w/w H_2O_2 and complete cell culture media (Dulbecco`s Modified Eagle Media (DMEM) supplemented with 10% fetal bovine serum (FBS)) at pH 4.56 and 7.54 (pH was adjusted with HCl/NaOH and confirmed by a pH meter) were tested for AuNS, AuNS-4MBA and AuNS-4MBA-PA, obtained from the same batch.

Characterization. TEM images were collected with a JEOL JEM-1400PLUS transmission electron microscope operating at 120 kV, using carbon coated 400 square mesh copper grids. UV-

Vis optical extinction spectra were recorded using an Agilent 8453 UV-Vis diode-array spectrophotometer. Dynamic UV-vis spectral monitoring was conducted by a Cary 3500 Multizone UV-vis spectrophotometer (Agilent Technologies, Inc.). Dynamic light scattering and zeta potential measurements were performed in a Malvern Zetasizer 3000 HS particle size analyzer (Malvern Instruments, UK). ICP-MS measurements were performed on a Thermo iCAP Q ICP-MS (Thermo Fisher Scientific GmbH, Bremen, Germany). An ASX-560 autosampler was coupled to the ICP-MS (CETAC Tech, Omaha,NE, USA). 2D SERS measurements were performed with a confocal Raman microscope (Renishaw inVia Reflex), equipped with 1024×512 CCD detectors using a 785 nm laser excitation source (maximum output 270 mW) and a 1200 l/mm diffraction grating. 3D SERS imaging was performed on a confocal Raman microscope (Witec alpha300R, WITec, Germany). The system is composed of a microscope (Zeiss), fiber-coupled laser excitation sources, piezo-driven scan platform (position accuracy 1 nm in x, y and 0.2 nm in z) and a 400 mm focal length imaging spectrometer (UHTS400) equipped with two gratings and a Peltier-cooled back-illuminated deep depletion CCD camera (1024×127px) optimized for NIR.

Protocol for pH calibration curve. The pH calibration curve was obtained in complete cell culture media (DMEM supplemented with 10% FBS). The pH of media was adjusted by addition of 1 M NaOH or HCl, and determined by an electronic pH meter (ThermoFisher) at room temperature. 50 μL of concentrated pH nanoprobe solution [Au^0= 3 mM] was added to 500 μL of each medium, fully mixed and transferred to a 96-well microplate for Raman measurements. The pH of each mixture was examined again by an electronic pH-meter to check the deviation caused by nanoparticle addition, which was below 0.05. The final Au concentration of AuNS-4MBA-PA was approximately 0.3 mM (~ 4.2×10^{10} NP mL^{-1}). The SERS signal of each mixture was

measured using a 785 nm laser (~30 mW), with 5 s exposure time and a 50× long working distance objective (numerical aperture N.A.=0.5), and the excitation laser spot focused in the middle of the well. Each sample was measured five times. The calibration curve of AuNS-4MBA (the concentration of 4MBA added to the NPs to fully functionalize them is ~20 molecules/nm^2, a 7-fold excess to theoretically reach a complete monolayer) was conducted in the same way and with the same measurement parameters as those used for AuNS-4MBA-PA.

Protocol for recall test and reversibility test

- The recall test was carried out to test the reliability of the pH probe. In this experiment, three aliquots of 2 mL of media with different pH were prepared and separated into two groups. In one group, the pH of media would be determined with AuNS-4MBA-PA by SERS, whereas in the other group, the pH was determined with an electronic pH meter.
- In the reversibility test, 0.3 mM AuNS-4MBA-PA colloidal solution (~ 4.2×10^{10} NP mL^{-1}) was prepared and a certain volume of 1M HCl added to adjust the pH around 4. Then, the same volume of 1M NaOH was added to change the pH toward neutral. The pH value was repeatedly varied between 4 and 7, and the SERS signal from the colloidal solution was measured after each pH change, using a 50× long working distance objective (NA=0.5), at a laser power of 30 mW with 2s exposure time.

Cell culture and viability tests. Human breast cancer cells (MCF7 cell line) were grown in DMEM supplemented with 10% FBS and 1% penicillin-streptomycin. Cells were cultured in a standard environment (humidified incubator with 5% CO_2 supplement at 37%). The MTT assay was conducted to evaluate the cytotoxicity of pH nanoprobes; MCF7 cells were seeded at a density

of 10^4 cells/well in a 96-well microplate and incubated for 24 h. Thereafter, media were replaced with 100 μL of fresh complete cell culture media containing different doses of pH nanoprobes. After incubation for 24 h, media were discarded and each well was washed twice with PBS buffer and 100 μL of fresh media containing 0.25 mg/mL MTT. After 1 h, the solution in each well was discarded again and the purple intracellular precipitate was dissolved in 100 μL of DMSO. After gently shaking, the optical density of the plate was read using a microplate reader with an excitation at 550 nm. Cells with media only served as a control group.

Cell sample preparation for ICP-MS. Cellular uptake of pH nanoprobes was quantified by ICP-MS. MCF7 cells were seeded in a 48-well microplate at a density of 2×10^4 cells/well and incubated for 24 h. Media was replaced with 200 μL of fresh media containing various concentrations of PA- or PEG-modified probes. After 24 h incubation, supernatants and cells were collected separately and frozen overnight to rupture the membranes. The following day, the samples were defrosted and dissolved in freshly prepared aqua regia for ICP-MS quantification.

Cell sample preparation for SERS measurements

Cellular uptake observation: MCF7 cells were seeded on quartz-bottom culture dishes (35 mm diameter) at a density of $5x10^4$ cells per dish and incubated for 24h for attachment. The medium was then replaced with complete medium containing 10 μg/mL AuNS-4MBA-PA ($\sim 7.0 \times 10^9$ NP mL^{-1}) and incubated for 2h. Afterwards, the supernatant was discarded and cells were gently washed with warm media three times to remove free nanoparticles, and immersed in fresh complete media for SERS measurements. When not being imaged, the cells were returned to the incubator. For 2D images, data collection was performed in *streamline mode* using a 40x water immersion objective (Nikon, N.A.= 0.8). In this mode, the laser was focused to a narrow line,

which allowed the generation of high definition 2D images with faster acquisition time than the spot mode. The total measurement time for each image was approximately 5 min. All (time-dependent) images were obtained at the same z position relative to the quartz bottom (using the inherent quartz signal to determine the 0 position). Raman spectra were acquired from 732.9 to 1816.7 cm^{-1} (center of scattered wavenumber was 1300 cm^{-1}). The laser power was ~ 6.5 mW (at surface) and exposure time was set to 2s.

3D Confocal Raman imaging. For 3D SERS experiments, the 785 nm excitation laser and a 63x water immersion objective (Zeiss) with N.A.=1.0 were used. SERS spectra were acquired with a 300 lines per mm grating, placed to the spectral center of 1499.816 $rel.cm^{-1}$ and the laser power set to 1.5 mW (measured with *True power* module corresponds to 0.9 mW at surface). Cells were imaged by collecting data from 7 layers of 2 μm increment in the z-axis. A 500 nm step size was used in the x and y axes for each SERS image, with 0.02 s integration time. The SERS probes and cell preparation were identical to those of 2D imaging. For each time point, the whole 3D data collection was completed within 2 hours and cells would be preserved in the incubation environment after imaging.

Data processing

In 2D imaging data, all hyper-spectral data were optimized by cosmic ray removal, baseline subtraction and smoothing, the functions provided by Renishaw software Wire 4.4. In the baseline subtraction, intelligent fitting mode with polynomial order of 11 was employed and noise tolerance was set as 1.5. Afterwards, spectra were smoothed by Savitzky-Golay filter with smooth window as 9. All spectra were processed under the same procedure with the same parameters before pH analysis. Thereafter, data were processed in batch by a homebuilt program through MATLAB

software (R2018a, MathWorks) for calibration curve generation, intensity ratio calculation as well as pH image reconstruction. As to intensity ratio calculation for pH indication, the absolute intensities at 1415, 1429 and 1081 cm^{-1} were read and calculated according to the equation below:

$$Ratio = \frac{I_{1415} + I_{1429}}{I_{1081}}$$

The correlation curves between pH and ratio were fit with Henderson-Hasselbalch Equation and generates the calibration curves for the pH sensor. In the pH map generation for cells, the spectrum of each pixel was optimized in the same way as described above. Before pH calculation, spectra were operated by a high-pass filter, which is generated according to the signal-to-noise ratio (SNR) of the spectrum (determination of SNR threshold is explained in supporting information **Figure S7**), so it can filter out the background and extract only the signal with valid information. The SNR of each spectrum was calculated by taking the highest intensity at 1081 cm^{-1} divided by the standard deviation of the noise from 1200 to 1300 cm^{-1}. Then, based on the calibration curve, the pH of each pixel was calculated and reconstructed.

For 3D data, all hyper-spectral data undergone cosmic ray removal, baseline correction and smoothing by the functions provided in WITec software Project FIVE 5.2 Plus. Afterwards, data were calculated layer by layer using a homebuilt program through MATLAB software (R2018a, MathWorks). pH reconstruction was conducted based on the same calibration curve as 2D data analysis.

ASSOCIATED CONTENT

Supporting Information Available: The following files are available free of charge.
SuppInfo.pdf. Detailed information about nanoparticle characterization, spectral analysis, Supporting Figures S1-S11 and Table S1.

AUTHOR INFORMATION

Corresponding Authors:

*E-mail: llizmarzan@cicbiomagune.es

*E-mail: djimenezdeaberasturi@cicbiomagune.es

Author Contributions

Y.Z, D.J.d.A. and M.H.L. designed the experiments. Y.Z performed the experiments and data analysis. J.L and Y.Z together performed the colloidal stability test and the SERS 3D imaging experiment. L.M.L.-M. conceived and supervised the project. The manuscript was written through contributions of all authors.

ACKNOWLEDGMENT

The authors acknowledge financial support from the European Research Council (ERC-AdG-2017# 787510). Y.Z acknowledges financial support from China Scholarship Council (CSC NO. 201806090115), Scientific Research Foundation of Graduate School of Southeast University (No. YBJJ1662) and the Postgraduate Research & Practice Innovation Program of Jiangsu Province (No. KYCX17_0063). This work was performed under the Maria de Maeztu Units of Excellence Program from the Spanish State Research Agency – Grant No. MDM-2017-0720. The authors acknowledge the comments and suggestions from Dr. Xiaolu Zhuo and Professor Yiping Cui.

REFERENCES

(1) Casey, J. R.; Grinstein, S.; Orlowski, J. Sensors and Regulators of Intracellular pH. *Nat. Rev. Mol. Cell Biol.* **2010**, *11* (1), 50–61. https://doi.org/10.1038/nrm2820.

(2) Puppulin, L.; Hosogi, S.; Sun, H.; Matsuo, K.; Inui, T.; Kumamoto, Y.; Suzaki, T.; Tanaka, H.; Marunaka, Y. Bioconjugation Strategy for Cell Surface Labelling with Gold

Nanostructures Designed for Highly Localized pH Measurement. *Nat. Commun.* **2018**, *9* (1), 5278. https://doi.org/10.1038/s41467-018-07726-5.

(3) Webb, B. A.; Chimenti, M.; Jacobson, M. P.; Barber, D. L. Dysregulated pH: A Perfect Storm for Cancer Progression. *Nat. Rev. Cancer* **2011**, *11* (9), 671–677. https://doi.org/10.1038/nrc3110.

(4) Zheng, X.; Hu, P.; Cui, Y.; Zong, C.; Feng, J.; Wang, X.; Ren, B. BSA-Coated Nanoparticles for Improved SERS-Based Intracellular pH Sensing. *Anal. Chem.* **2014**, *86* (24), 12250–12257. https://doi.org/10.1021/ac503404u.

(5) Wei, H.; Vejerano, E. P.; Leng, W.; Huang, Q.; Willner, M. R.; Marr, L. C.; Vikesland, P. J. Aerosol Microdroplets Exhibit a Stable pH Gradient. *Proc. Natl. Acad. Sci.* **2018**, *115* (28), 7272–7277. https://doi.org/10.1073/pnas.1720488115.

(6) Zheng, X.; Zong, C.; Wang, X.; Ren, B. Cell-Penetrating Peptide Conjugated SERS Nanosensor for in Situ Intracellular pH Imaging of Single Living Cells during Cell Cycle. *Anal. Chem.* **2019**, *91* (13), 8383–8389. https://doi.org/10.1021/acs.analchem.9b01191.

(7) Park, J. E.; Yonet-Tanyeri, N.; Vander Ende, E.; Henry, A.-I.; Perez White, B. E.; Mrksich, M.; Van Duyne, R. P. Plasmonic Microneedle Arrays for in Situ Sensing with Surface-Enhanced Raman Spectroscopy (SERS). *Nano Lett.* **2019**, *19* (10), 6862–6868. https://doi.org/10.1021/acs.nanolett.9b02070.

(8) Jimenez de Aberasturi, D.; Henriksen-Lacey, M.; Litti, L.; Langer, J.; Liz-Marzán, L. M. Using SERS Tags to Image the Three-Dimensional Structure of Complex Cell Models. *Adv. Funct. Mater.* **2020**, *30* (14), 1909655. https://doi.org/10.1002/adfm.201909655.

(9) Lenzi, E.; Jimenez de Aberasturi, D.; Liz-Marzán, L. M. Surface-Enhanced Raman Scattering Tags for Three-Dimensional Bioimaging and Biomarker Detection. *ACS Sensors* **2019**, *4* (5), 1126–1137. https://doi.org/10.1021/acssensors.9b00321.

(10) Jimenez De Aberasturi, D.; Serrano-Montes, A. B.; Langer, J.; Henriksen-Lacey, M.; Parak, W. J.; Liz-Marzán, L. M. Surface Enhanced Raman Scattering Encoded Gold Nanostars for Multiplexed Cell Discrimination. *Chem. Mater.* **2016**, *28* (18), 6779–6790. https://doi.org/10.1021/acs.chemmater.6b03349.

(11) Langer, J.; Jimenez de Aberasturi, D.; Aizpurua, J.; Alvarez-Puebla, R. A.; Auguié, B.; Baumberg, J. J.; Bazan, G. C.; Bell, S. E. J.; Boisen, A.; Brolo, A. G.; et al. Present and Future of Surface-Enhanced Raman Scattering. *ACS Nano* **2020**, *14* (1), 28–117. https://doi.org/10.1021/acsnano.9b04224.

(12) Pallaoro, A.; Braun, G. B.; Reich, N. O.; Moskovits, M. Mapping Local pH in Live Cells Using Encapsulated Fluorescent SERS Nanotags. *Small* **2010**, *6* (5), 618–622. https://doi.org/10.1002/smll.200901893.

(13) Capocefalo, A.; Mammucari, D.; Brasili, F.; Fasolato, C.; Bordi, F.; Postorino, P.; Domenici, F. Exploring the Potentiality of a SERS-Active pH Nano-Biosensor. *Front. Chem.* **2019**, *7* (6), 1–11. https://doi.org/10.3389/fchem.2019.00413.

(14) Xu, M.; Ma, X.; Wei, T.; Lu, Z. X.; Ren, B. In Situ Imaging of Live-Cell Extracellular pH during Cell Apoptosis with Surface-Enhanced Raman Spectroscopy. *Anal. Chem.* **2018**, *90* (23), 13922–13928. https://doi.org/10.1021/acs.analchem.8b03193.

(15) Shen, Y.; Liang, L.; Zhang, S.; Huang, D.; Zhang, J.; Xu, S.; Liang, C.; Xu, W. Organelle-Targeting Surface-Enhanced Raman Scattering (SERS) Nanosensors for Subcellular pH Sensing. *Nanoscale* **2018**, *10* (4), 1622–1630. https://doi.org/10.1039/c7nr08636a.

(16) Kallepitis, C.; Bergholt, M. S.; Mazo, M. M.; Leonardo, V.; Skaalure, S. C.; Maynard, S. A.; Stevens, M. M. Quantitative Volumetric Raman Imaging of Three Dimensional Cell Cultures. *Nat. Commun.* **2017**, *8* (1), 14843. https://doi.org/10.1038/ncomms14843.

(17) McAughtrie, S.; Lau, K.; Faulds, K.; Graham, D. 3D Optical Imaging of Multiple SERS Nanotags in Cells. *Chem. Sci.* **2013**, *4* (9), 3566–3572. https://doi.org/10.1039/c3sc51437d.

(18) Kapara, A.; Brunton, V.; Graham, D.; Faulds, K. Investigation of Cellular Uptake Mechanism of Functionalised Gold Nanoparticles into Breast Cancer Using SERS. *Chem. Sci.* **2020**, *11* (22), 5819–5829. https://doi.org/10.1039/D0SC01255F.

(19) Huang, K. C.; Bando, K.; Ando, J.; Smith, N. I.; Fujita, K.; Kawata, S. 3D SERS (Surface Enhanced Raman Scattering) Imaging of Intracellular Pathways. *Methods* **2014**, *68* (2), 348–353. https://doi.org/10.1016/j.ymeth.2014.02.007.

(20) Ando, J.; Fujita, K.; Smith, N. I.; Kawata, S. Dynamic SERS Imaging of Cellular Transport Pathways with Endocytosed Gold Nanoparticles. *Nano Lett.* **2011**, *11* (12), 5344–5348. https://doi.org/10.1021/nl202877r.

(21) Bando, K.; Zhang, Z.; Graham, D.; Faulds, K.; Fujita, K.; Kawata, S. Dynamic pH Measurements of Intracellular Pathways Using Nano-Plasmonic Assemblies. *Analyst* **2020**. https://doi.org/10.1039/D0AN00986E.

(22) Bishnoi, S. W.; Rozell, C. J.; Levin, C. S.; Gheith, M. K.; Johnson, B. R.; Johnson, D. H.; Halas, N. J. All-Optical Nanoscale pH Meter. *Nano Lett.* **2006**, *6* (8), 1687–1692. https://doi.org/10.1021/nl060865w.

(23) Sun, F.; Zhang, P.; Bai, T.; David Galvan, D.; Hung, H.-C.; Zhou, N.; Jiang, S.; Yu, Q. Functionalized Plasmonic Nanostructure Arrays for Direct and Accurate Mapping Extracellular pH of Living Cells in Complex Media Using SERS. *Biosens. Bioelectron.* **2015**, *73*, 202–207. https://doi.org/10.1016/j.bios.2015.05.060.

(24) Jaworska, A.; Jamieson, L. E.; Malek, K.; Campbell, C. J.; Choo, J.; Chlopicki, S.; Baranska, M. SERS-Based Monitoring of the Intracellular pH in Endothelial Cells: The Influence of the Extracellular Environment and Tumour Necrosis Factor-α. *Analyst* **2015**, *140* (7), 2321–2329. https://doi.org/10.1039/c4an01988a.

(25) Zhang, Z.; Bando, K.; Mochizuki, K.; Taguchi, A.; Fujita, K.; Kawata, S. Quantitative Evaluation of Surface-Enhanced Raman Scattering Nanoparticles for Intracellular pH Sensing at a Single Particle Level. *Anal. Chem.* **2019**, *91* (5), 3254–3262. https://doi.org/10.1021/acs.analchem.8b03276.

(26) Zong, S.; Wang, Z.; Yang, J.; Cui, Y. Intracellular pH Sensing Using P-Aminothiophenol Functionalized Gold Nanorods with Low Cytotoxicity. *Anal. Chem.* **2011**, *83* (11), 4178–4183. https://doi.org/10.1021/ac200467z.

(27) Alvarez-Puebla, R. A.; Liz-Marzán, L. M. SERS Detection of Small Inorganic Molecules and Ions. *Angew. Chemie - Int. Ed.* **2012**, *51* (45), 11214–11223. https://doi.org/10.1002/anie.201204438.

(28) Pastoriza-Santos, I.; Kinnear, C.; Pérez-Juste, J.; Mulvaney, P.; Liz-Marzán, L. M. Plasmonic Polymer Nanocomposites. *Nat. Rev. Mater.* **2018**, *3* (10), 375–391. https://doi.org/10.1038/s41578-018-0050-7.

(29) Zhai, W.; He, C.; Wu, L.; Zhou, Y.; Chen, H.; Chang, J.; Zhang, H. Degradation of Hollow Mesoporous Silica Nanoparticles in Human Umbilical Vein Endothelial Cells. *J. Biomed. Mater. Res. Part B Appl. Biomater.* **2012**, *100B* (5), 1397–1403. https://doi.org/10.1002/jbm.b.32711.

(30) Hao, N.; Liu, H.; Li, L.; Chen, D.; Li, L.; Tang, F. In Vitro Degradation Behavior of Silica Nanoparticles Under Physiological Conditions . *J. Nanosci. Nanotechnol.* **2012**, *12* (8), 6346–6354. https://doi.org/10.1166/jnn.2012.6199.

(31) Chen, G.; Teng, Z.; Su, X.; Liu, Y.; Lu, G. Unique Biological Degradation Behavior of Stöber Mesoporous Silica Nanoparticles from Their Interiors to Their Exteriors. *J. Biomed. Nanotechnol.* **2015**, *11* (4), 722–729. https://doi.org/10.1166/jbn.2015.2072.

(32) Li, R.; Wu, Z.; Wangb, Y.; Ding, L.; Wang, Y. Role of pH-Induced Structural Change in Protein Aggregation in Foam Fractionation of Bovine Serum Albumin. *Biotechnol. Reports* **2016**, *9*, 46–52. https://doi.org/10.1016/j.btre.2016.01.002.

(33) Ishikawa, M.; Biju, V. *Luminescent Quantum Dots, Making Invisibles Visible in Bioimaging*, 1st ed.; Elsevier Inc., 2011; Vol. 104. https://doi.org/10.1016/B978-0-12-416020-0.00002-4.

(34) Mitchell, D. J.; Steinman, L.; Kim, D. T.; Fathman, C. G.; Rothbard, J. B. Polyarginine Enters Cells More Efficiently than Other Polycationic Homopolymers. *J. Pept. Res.* **2000**, *56* (5), 318–325. https://doi.org/10.1034/j.1399-3011.2000.00723.x.

(35) Yuan, H.; Khoury, C. G.; Hwang, H.; Wilson, C. M.; Grant, G. A.; Vo-Dinh, T. Gold Nanostars: Surfactant-Free Synthesis, 3D Modelling, and Two-Photon Photoluminescence Imaging. *Nanotechnology* **2012**, *23* (7). https://doi.org/10.1088/0957-4484/23/7/075102.

(36) Vega, M. M.; Bonifacio, A.; Lughi, V.; Marsi, S.; Carrato, S.; Sergo, V. Long-Term Stability of Surfactant-Free Gold Nanostars. *J. Nanoparticle Res.* **2014**, *16* (11), 2729. https://doi.org/10.1007/s11051-014-2729-z.

(37) Abdal Dayem, A.; Hossain, M.; Lee, S.; Kim, K.; Saha, S.; Yang, G.; Choi, H.; Cho, S. The Role of Reactive Oxygen Species (ROS) in the Biological Activities of Metallic Nanoparticles. *Int. J. Mol. Sci.* **2017**, *18* (1), 120. https://doi.org/10.3390/ijms18010120.

(38) Kumari, S.; Badana, A. K.; Murali Mohan, G.; Shailender, G.; Malla, R. R. Reactive Oxygen Species: A Key Constituent in Cancer Survival. *Biomark. Insights* **2018**, *13*, 117727191875539. https://doi.org/10.1177/1177271918755391.

(39) Ma, Y.; Zhu, Y.; Liu, B.; Quan, G.; Cui, L. Colorimetric Determination of Hypochlorite Based on the Oxidative Leaching of Gold Nanorods. *Materials (Basel).* **2018**, *11* (9), 9–14. https://doi.org/10.3390/ma11091629.

(40) Wen, T.; Zhang, H.; Tang, X.; Chu, W.; Liu, W.; Ji, Y.; Hu, Z.; Hou, S.; Hu, X.; Wu, X. Copper Ion Assisted Reshaping and Etching of Gold Nanorods: Mechanism Studies and Applications. *J. Phys. Chem. C* **2013**, *117* (48), 25769–25777. https://doi.org/10.1021/jp407774s.

(41) Mulder, D.; Phiri, M. M.; Vorster, B. C. Tailor-Made Gold Nanostar Colorimetric Detection Determined by Morphology Change and Used as an Indirect Approach by Using Hydrogen Peroxide to Determine Glucose Concentration. *Sens. Bio-Sensing Res.* **2019**, *25* (April), 100296. https://doi.org/10.1016/j.sbsr.2019.100296.

(42) Manke, A.; Wang, L.; Rojanasakul, Y. Mechanisms of Nanoparticle-Induced Oxidative Stress and Toxicity. *Biomed Res. Int.* **2013**, *2013*, 1–15. https://doi.org/10.1155/2013/942916.

(43) Cui, K.; Fan, C.; Chen, G.; Qiu, Y.; Li, M.; Lin, M.; Wan, J.-B.; Cai, C.; Xiao, Z. Para -Aminothiophenol Radical Reaction-Functionalized Gold Nanoprobe for One-to-All Detection of Five Reactive Oxygen Species In Vivo. *Anal. Chem.* **2018**, *90* (20), 12137–12144. https://doi.org/10.1021/acs.analchem.8b03116.

(44) Wang, Y.; Serrano, A. B.; Sentosun, K.; Bals, S.; Liz-Marzán, L. M. Stabilization and Encapsulation of Gold Nanostars Mediated by Dithiols. *Small* **2015**, *11* (34), 4314–4320. https://doi.org/10.1002/smll.201500703.

(45) Kozin, L. F.; Prokopenko, V. A.; Bogdanova, A. K. Kinetics and Mechanism of the Gold Corrosion Dissolution in Hypochlorite Solutions. *Prot. Met.* **2005**, *41* (1), 22–29. https://doi.org/10.1007/s11124-005-0003-6.

(46) Casals, E.; Pfaller, T.; Duschl, A.; Oostingh, G. J.; Puntes, V. Time Evolution of the Nanoparticle Protein Corona. *ACS Nano* **2010**, *4* (7), 3623–3632. https://doi.org/10.1021/nn901372t.

(47) Docter, D.; Westmeier, D.; Markiewicz, M.; Stolte, S.; Knauer, S. K.; Stauber, R. H. The Nanoparticle Biomolecule Corona: Lessons Learned – Challenge Accepted? *Chem. Soc. Rev.* **2015**, *44* (17), 6094–6121. https://doi.org/10.1039/C5CS00217F.

(48) Moore, T. L.; Urban, D. A.; Rodriguez-Lorenzo, L.; Milosevic, A.; Crippa, F.; Spuch-Calvar, M.; Balog, S.; Rothen-Rutishauser, B.; Lattuada, M.; Petri-Fink, A. Nanoparticle Administration Method in Cell Culture Alters Particle-Cell Interaction. *Sci. Rep.* **2019**, *9* (1), 900. https://doi.org/10.1038/s41598-018-36954-4.

(49) Li, S.; Zhang, M.; Wang, J.; Yang, F.; Kang, B.; Xu, J.; Chen, H. Monitoring the Changes of pH in Lysosomes during Autophagy and Apoptosis by Plasmon Enhanced Raman Imaging. *Anal. Chem.* **2019**, *91* (13), 8398–8405. https://doi.org/10.1021/acs.analchem.9b01250.

(50) Ho, C.-H.; Lee, S. SERS and DFT Investigation of the Adsorption Behavior of 4-Mercaptobenzoic Acid on Silver Colloids. *Colloids Surfaces A Physicochem. Eng. Asp.* **2015**, *474*, 29–35. https://doi.org/10.1016/j.colsurfa.2015.03.004.

(51) Phan, H. T.; Haes, A. J. Impacts of pH and Intermolecular Interactions on Surface-Enhanced Raman Scattering Chemical Enhancements. *J. Phys. Chem. C* **2018**, *122* (26), 14846–14856. https://doi.org/10.1021/acs.jpcc.8b04019.

(52) Serrano-Montes, A. B.; Langer, J.; Henriksen-Lacey, M.; Jimenez De Aberasturi, D.; Solís, D. M.; Taboada, J. M.; Obelleiro, F.; Sentosun, K.; Bals, S.; Bekdemir, A.; et al. Gold Nanostar-Coated Polystyrene Beads as Multifunctional Nanoprobes for SERS Bioimaging. *J. Phys. Chem. C* **2016**, *120* (37), 20860–20868. https://doi.org/10.1021/acs.jpcc.6b02282.

(53) Carnevale, K. J. F.; Riskowski, R. A.; Strouse, G. F. A Gold Nanoparticle Bio-Optical Transponder to Dynamically Monitor Intracellular pH. *ACS Nano* **2018**, *12* (6), 5956–5968. https://doi.org/10.1021/acsnano.8b02200.

(54) Chou, L. Y. T.; Ming, K.; Chan, W. C. W. Strategies for the Intracellular Delivery of Nanoparticles. *Chem. Soc. Rev.* **2011**, *40* (1), 233–245. https://doi.org/10.1039/c0cs00003e.

(55) Huotari, J.; Helenius, A. Endosome Maturation. *EMBO J.* **2011**, *30* (17), 3481–3500. https://doi.org/10.1038/emboj.2011.286.

(56) Foroozandeh, P.; Aziz, A. A. Insight into Cellular Uptake and Intracellular Trafficking of Nanoparticles. *Nanoscale Res. Lett.* **2018**, *13* (1), 339. https://doi.org/10.1186/s11671-018-2728-6.

(57) Leporatti, S.; Vergara, D.; Zacheo, A.; Vergaro, V.; Maruccio, G.; Cingolani, R.; Rinaldi, R. Cytomechanical and Topological Investigation of MCF-7 Cells by Scanning Force Microscopy. *Nanotechnology* **2009**, *20* (5), 055103. https://doi.org/10.1088/0957-4484/20/5/055103.

(58) Sisco, P. N.; Murphy, C. J. Surface-Coverage Dependence of Surface-Enhanced Raman Scattering from Gold Nanocubes on Self-Asssembled Monolayers of Analyte. *J. Phys. Chem. A* **2009**, *113* (16), 3973–3978. https://doi.org/10.1021/jp810329j.

For TOC only

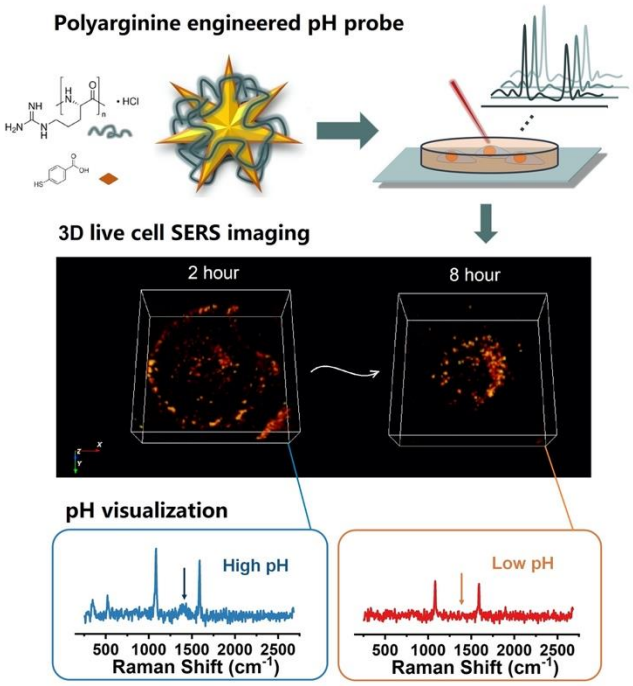
Polyarginine engineered pH probe
3D live cell SERS imaging
2 hour
8 hour
pH visualization
High pH
Low pH
500 1000 1500 2000 2500
Raman Shift (cm-1)
500 1000 1500 2000 2500
Raman Shift (cm-1)